



Research papers

Localisation of coastal trapped waves by longshore variations in bottom topography

J.T. Rodney*, E.R. Johnson

University College London, Department of Mathematics, Gower Street, London WC1E 6BT, United Kingdom

ARTICLE INFO

Article history:

Received 17 June 2011

Received in revised form

19 October 2011

Accepted 2 November 2011

Available online 20 November 2011

Keywords:

Trapped modes

Coastal trapped waves

WKB approximation

ABSTRACT

Variations in shelf geometry mean that a coastal trapped wave mode can propagate within some finite length of shelf but be evanescent outside this region. This paper constructs such geographically localised coastal trapped waves using a WKB approximation. Comparison with full numerical solutions of the non-linear differential eigenvalue problem demonstrates that the approximation is extremely accurate. The asymptotic and full numerical models are then used to examine the parameters and geometries that govern the existence of these modes.

© 2011 Published by Elsevier Ltd.

1. Introduction

Sub-inertial disturbances confined over stratified continental shelves are generally described as coastal trapped waves (CTWs). The properties of CTWs are closely related to a merging of the internal Kelvin wave and barotropic continental shelf wave limits, and the waves can typically be regarded as a hybrid of the two. Most theoretical discussions of CTWs are based on the assumption that the coast and shelf profile are uniform in the longshore direction. However in practice there may be significant longshore variations in shelf depth profiles and coastline curvature. These longshore variations can give rise to regions of localised wave propagation with modes decaying outside these regions in both the longshore and offshore directions. These localised disturbances will be denoted here as localised CTWs (ℓ CTWs). As energy at the ℓ CTW frequency is trapped within a fixed section of the shelf such modes could be resonantly excited by broadband forcing from wind fluctuating and interacting with offshore eddies, and so could appear preferentially as peaks in the low-frequency coastal energy spectra (Schwing, 1989; Stocker and Johnson, 1991).

Johnson et al. (2006) prove that localised continental shelf waves (ℓ CTWs) can exist on smoothly curving coastlines, Postnova and Craster (2008) present an asymptotic method for determining the frequencies of ℓ CTWs on slowly curving coastlines, discussed in greater detail in Johnson et al. (2011), and Kaoullas and Johnson (2010) construct ℓ CTWs for an idealised model of a curved coast using a semi-analytical mode-matching technique. All these studies restrict attention to barotropic flow

and use an approximate Neumann boundary condition at the shelf ocean boundary. The localisation of the modes is closely related to the behaviour of the group velocity and relies on bi-directional energy propagation in the localisation region. Huthnance (1978) shows that, in general, increasing stratification changes bi-directional propagation to purely uni-directional propagation. At sufficiently high stratifications localisation is thus impossible.

The aim of this paper is to examine the effect of variations in stratification, alongshore shelf slope and alongshore shelf width on ℓ CTWs. Geographically localised CTWs are constructed asymptotically using a WKB approach in Section 3 to give a resonance condition for the ℓ CTW frequencies. The WKB approximation appears here in the longshore direction in contrast to previous applications in oceanography when modes decay in the offshore direction only (e.g. in Adamou et al., 2007 in their discussion of trapped edge waves in the internal gravity wave band). In Section 4 ℓ CTWs are computed using a 3D extension to the highly accurate 2D spectral numerical scheme of Johnson and Rodney (2011) (JR here). Section 5 demonstrates the importance of stratification, shelf slope and shelf-break distance from the coastal wall on ℓ CTWs. Neither the asymptotic nor the numerical methods presented here require any approximate offshore boundary condition and their close agreement demonstrates the extreme accuracy of the WKB model in the present problem.

2. Formulation

Consider a rotating incompressible ocean with uniform Coriolis frequency f . Take Cartesian axis Ox, Oy, Oz along the shelf, out to sea

* Corresponding author.

E-mail addresses: j.rodney@ucl.ac.uk, jamier@math.ucl.ac.uk (J.T. Rodney).

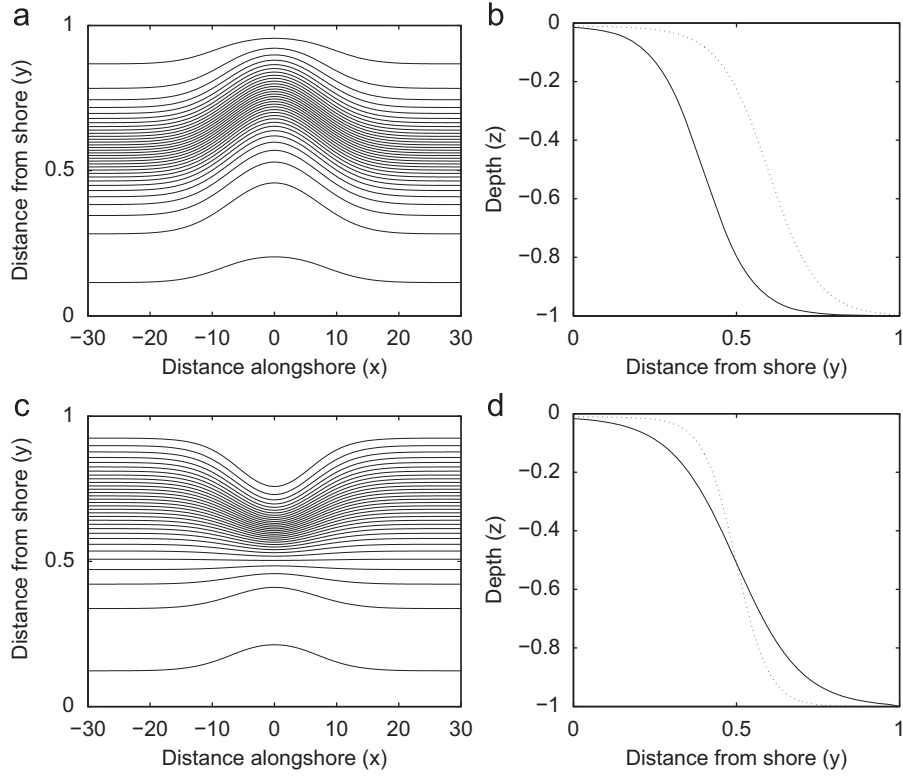


Fig. 1. Isobaths and depth profiles of (a,b) the shelf with local perturbation in shelf-break distance given by (54) with $H_0 = 0.01$, $a = 0.01$, $\sigma = 0.4 + 0.2 \exp\{-(\varepsilon x)^2\}$ and $\delta = 0.15$, (c,d) the shelf with local perturbation in shelf slope given by (54) with $H_0 = 0.01$, $a = 0.01$, $\sigma = 0.5$ and $\delta = 0.2 - 0.1 \exp\{-(\varepsilon x)^2\}$. In (b,d) the solid line is the unperturbed far field profile and the dashed line gives the maximally perturbed profile (at $x=0$).

and vertical with the shelf profile depending on both x and y (Fig. 1). Let the flow be Boussinesq with total density $\rho_0(z) + \rho(x,y,z,t)$ and pressure $p_0(z) + p(x,y,z,t)$. The equilibrium values ρ_0 and p_0 are in hydrostatic balance, i.e. $\partial p_0 / \partial z = \rho_0 g$. Introduce the buoyancy frequency $\mathcal{N}^2 = -(g/\rho_0) d\rho_0/dz$, and scalings

$$(x', y', z') = (x/L, y/L, z/H), \quad (u', v', w') = (u/U, v/U, wL/UH),$$

$$p' = p/\rho_0(0)fUL, \quad \rho' = \rho gH/\rho_0(0)fUL, \quad \mathcal{N}'(z) = \mathcal{N}_0 b(z), \quad (1)$$

where L is the shelf width, H deep sea depth, U typical horizontal velocity, f the Coriolis parameter and \mathcal{N}_0 is the maximum buoyancy frequency. The non-dimensional equations for a normal mode of non-dimensional frequency ω in the body of the fluid are then, dropping the primes and omitting a common exponential factor $\exp\{-i\omega t\}$

$$-i\omega u - v = -p_x, \quad (2)$$

$$-i\omega v + u = -p_y, \quad (3)$$

$$-p_z - \rho = 0, \quad (4)$$

$$u_x + v_y + w_z = 0, \quad (5)$$

$$-i\omega \rho - b^2 B^2 w = 0, \quad (6)$$

where, for the ease of exposition, the perturbation has been taken to be hydrostatic. The non-dimensional parameter $B = \mathcal{N}_0 H / fL$ measures the importance of stratification relative to the rotation of the dynamics. Eqs. (2), (3), (5) and (6) combine to give the velocity components in terms of the pressure alone as

$$u = (-p_y + i\omega p_x) / (1 - \omega^2), \quad v = (p_x + i\omega p_y) / (1 - \omega^2), \quad (7)$$

$$w = (i\omega / b^2 B^2) p_z.$$

The vanishing of the normal component of velocity on the bottom and coastal boundaries gives

$$v = 0 \quad (y = 0), \quad (8)$$

$$w = -u\hat{h}_x - v\hat{h}_y \quad (z = -\hat{h}(x,y), y \leq 1). \quad (9)$$

For typical shelves the external Rossby deformation radius \sqrt{gH}/f is large compared to the shelf width, so the ocean surface is effectively rigid, and the upper boundary condition is simply the vanishing of the vertical velocity, i.e. the “rigid lid” boundary condition

$$p_z = 0 \quad (z = 0). \quad (10)$$

Surface deformation can be important over wide shelves, when the external Rossby deformation radius is comparable to or smaller than the shelf width, i.e. $\hat{a} = \sqrt{gH}/fL$ is of order unity or smaller, and then (10) becomes $p_z + (Bb(0)/\hat{a})^2 p = 0$. The extension of the present results to this case follows immediately from JR.

For disturbances of finite energy, it is sufficient to require

$$\nabla p \rightarrow 0, \quad x^2 + y^2 \rightarrow \infty, \quad (11)$$

as then, from (7), all velocity components vanish (exponentially fast) at infinity.

3. Slowly varying shelf geometry

Suppose the offshore profile of shelf depth changes only slowly with distance along the shelf, i.e. that $\hat{h}(x,y) = h(\varepsilon x,y) = h(\xi,y)$ where ε is a small dimensionless parameter representing the ratio of the shelf width to the scale of the longitudinal variation in offshore depth profile. Substituting for u, v, w in (5), (8), (9) gives

$$\varepsilon^2 p_{\xi\xi} + p_{yy} + (1 - \omega^2) B^{-2} (b^{-2} p_z)_z = 0, \quad (12a)$$

$$i\omega(1-\omega^2)b^{-2}B^{-2}p_z = -\varepsilon h_\xi(\varepsilon i\omega p_\xi - p_y) - h_y(\varepsilon p_\xi + i\omega p_y) \quad (12b)$$

$$(z = -h(\xi, y), y \leq 1),$$

$$\varepsilon p_\xi + i\omega p_y = 0 \quad (y = 0), \quad (12c)$$

$$p_z = 0 \quad (z = -1, y > 1), \quad (12d)$$

$$p_z = 0 \quad (z = 0), \quad (12e)$$

$$\nabla p \rightarrow 0, \quad \xi^2 + y^2 \rightarrow \infty. \quad (12f)$$

Consider the classical WKBJ ansatz

$$p(\xi, y, z) \sim \exp(iS(\xi)/\varepsilon) \sum_{j=0}^{\infty} \varepsilon^j \psi_j(\xi, y, z), \quad (13)$$

in which only the amplitude is expanded in powers of ε . Substituting (13) into (12) leads to a hierarchy of equations, the lowest order of which, of order ε^0 , gives

$$\psi_{0yy} + (1-\omega^2)B^{-2}(b^{-2}\psi_{0z})_z - S'^2\psi_0 = 0, \quad (14a)$$

$$\omega(1-\omega^2)b^{-2}B^{-2}\psi_{0z} = -S'h_y\psi_0 - \omega h_y\psi_{0y} \quad (z = -h(\xi, y), y \leq 1), \quad (14b)$$

$$\omega\psi_{0y} + S'\psi_0 = 0 \quad (y = 0), \quad (14c)$$

$$\psi_{0z} = 0 \quad (z = -1, y > 1), \quad (14d)$$

$$\psi_{0z} = 0 \quad (z = 0), \quad (14e)$$

$$\psi_0 \rightarrow 0 \quad y \rightarrow \infty \quad (14f)$$

and the next order, of order ε , gives

$$\psi_{1yy} + (1-\omega^2)B^{-2}(b^{-2}\psi_{1z})_z - S'^2\psi_1 = -2iS'\psi_{0\xi} - iS''\psi_0, \quad (15a)$$

$$i\omega(1-\omega^2)b^{-2}B^{-2}\psi_{1z} = -iS'h_y\psi_1 - i\omega h_y\psi_{1y} + h_y\psi_{0\xi} + h_\xi\psi_{0y} - \omega S'h_\xi\psi_0 \quad (z = -h(\xi, y), y \leq 1), \quad (15b)$$

$$i\omega\psi_{1y} + iS'\psi_1 + \psi_{0\xi} = 0 \quad (y = 0), \quad (15c)$$

$$\psi_{1z} = 0 \quad (z = -1, y > 1), \quad (15d)$$

$$\psi_{1z} = 0 \quad (z = 0), \quad (15e)$$

$$\psi_1 \rightarrow 0, \quad y \rightarrow \infty. \quad (15f)$$

System (14) is precisely the system that would determine the local dispersion relation at each station $x = \text{constant}$ along the shelf if the shelf were taken to be rectilinear of fixed offshore profile. For a given frequency the dispersion relation determines a local wavenumber k as a function of ξ . Fig. 2 gives typical dispersion curves for the shelf topography of Fig. 1(a,b) (both figures discussed in detail later). Fig. 2 shows that for each cross-shelf mode, for the parameter values chosen here, there is a local cut off frequency $\omega_{\max}(\xi)$, such that for $\omega < \omega_{\max}(\xi)$ there are two roots k^\pm for the wavenumber, corresponding to energy propagation in the positive and negative x -directions. Once the frequency exceeds ω_{\max} for a given cross-shelf mode, the wavenumbers k^\pm form a complex conjugate pair and the modes are evanescent. At the cut off frequency $\partial\omega/\partial k = 0$, the group velocity vanishes, and the wavenumbers k^- and k^+ coalesce.

Let $\phi^\pm(\xi, y, z)$ be the local eigenmodes, with corresponding eigenvalues $k^\pm(\xi)$ of the following problem in the cross section $\mathcal{D}(\xi) = \{(y, z) : -h(\xi, y) \leq z \leq 0, y \geq 0\}$

$$\phi_{yy}^\pm + (1-\omega^2)B^{-2}(b^{-2}\phi_z^\pm)_z = k^{\pm 2}\phi^\pm, \quad (16)$$

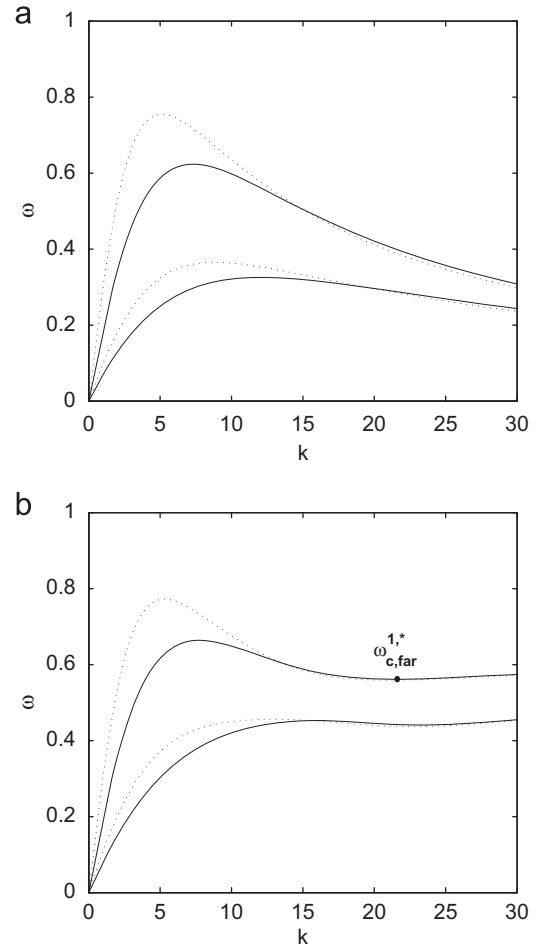


Fig. 2. Dispersion curves for modes 1 and 2 over the far shelf break (dashed line) and close shelf break (solid line) for the depth profiles shown in Fig. 1(a,b) at uniform stratification with (a) $B=0.01$ and (b) $B=0.2$.

$$\omega(1-\omega^2)b^{-2}B^{-2}\phi_z^\pm + \omega h_y\phi_y^\pm = -k^\pm h_y\phi^\pm \quad (z = -h(\xi, y), y \leq 1), \quad (17)$$

$$\omega\phi_y^\pm = -k^\pm\phi^\pm \quad (y = 0), \quad (18)$$

$$\phi_z^\pm = 0 \quad (z = -1), \quad (19)$$

$$\phi_z^\pm = 0 \quad (z = 0), \quad (20)$$

$$\phi^\pm \rightarrow 0, \quad y \rightarrow \infty, \quad (21)$$

where, for convenience, ϕ^\pm are normalised such that

$$\iint_{\mathcal{D}} (\phi^\pm)^2 dy dz = 1. \quad (22)$$

It follows that ψ_0^\pm can be expressed as an undetermined multiple of the local eigenmodes ϕ^\pm , i.e.

$$\psi_0^\pm(\xi, y, z) = f_0^\pm(\xi)\phi^\pm(\xi, y, z). \quad (23)$$

The function S' can then be identified with the two roots $k^\pm(\xi)$ for the wavenumber. Writing $S^\pm(\xi) = l(\xi) \pm m(\xi)$ gives

$$l(\xi) = \frac{1}{2} \int_{\xi_0}^{\xi} [k^+(\xi') + k^-(\xi')] d\xi', \quad (24)$$

$$m(\xi) = \frac{1}{2} \int_{\xi_0}^{\xi} [k^+(\xi') - k^-(\xi')] d\xi'. \quad (25)$$

Here l is the (fast) phase of each wave, which remains the same for the forward and backward propagating modes defined by S^+ and S^- , and m gives the direction of propagation of the wave envelope (and thus energy propagation), becoming singular at the caustic, defined by $k^+ = k^-$. The lower limit of integration in (25), the ‘phase reference level’ (Heading, 1962; Berry and Mount, 1972), is determined by the location of the caustic.

It is not necessary to solve (15) completely to obtain the eigenfrequencies. Multiplying (15a) by ϕ , integrating over the domain \mathcal{D} , and using the boundary conditions (14b)–(14f) and (15b)–(15f) gives the transport equation for the functions f_0^\pm

$$(A^\pm + B^\pm - 2\omega S^{\pm'})f_{0\xi}^\pm + (C^\pm - D^\pm + E^\pm - \omega S^{\pm'})f_0^\pm = 0, \quad (26)$$

where

$$A^\pm(\xi) = \int_0^1 h_y[\phi^{\pm 2}]_{z=-h} dy, \quad B^\pm(\xi) = \int_{-h_0}^0 [\phi^{\pm 2}]_{y=0} dz,$$

$$C^\pm(\xi) = \int_0^1 h_y[\phi_\xi^\pm \phi^\pm]_{z=-h} dy, \quad D^\pm(\xi) = \int_0^1 h_\xi[\phi_y^\pm \phi^\pm]_{z=-h} dy,$$

$$E^\pm(\xi) = \int_{-h_0}^0 [\phi^\pm \phi_\xi^\pm]_{y=0} dz.$$

The term $C^\pm - D^\pm$ can be rewritten as

$$C^\pm - D^\pm = \frac{1}{2} \frac{dA^\pm}{d\xi} + G^\pm, \quad (27)$$

where $G^\pm(\xi) = h_\xi(\xi, 0)\phi^{\pm 2}(\xi, 0, -h(\xi, 0)) - h_\xi(\xi, 1)\phi^{\pm 2}(\xi, 1, -h(\xi, 1))$. Provided the depth at the coast and the shelf-ocean boundary remains constant $h_\xi(\xi, 1) = h_\xi(\xi, 0) = 0$, and so $G^\pm(\xi) = 0$. Then (26) becomes

$$f_{0\xi}^\pm + \left[\frac{\frac{1}{2}(A^\pm + B^\pm - 2\omega S^{\pm'})_\xi}{A^\pm + B^\pm - 2\omega S^{\pm'}} \right] f_0^\pm = 0. \quad (28)$$

Eq. (28) is an ordinary differential equation for $f_0^\pm(\xi)$, with solution, to within an arbitrary multiplicative constant

$$f_0^\pm(\xi) = (A^\pm + B^\pm - 2\omega S^{\pm'})^{-1/2}. \quad (29)$$

An expression for the group velocities C_g^\pm of the propagating wave solutions of (16) follows by multiplying (16) by ϕ^\pm and integrating over the domain $D(\xi)$, to give

$$A^\pm + B^\pm - 2\omega k^\pm = C_g^\pm \tilde{I}^\pm, \quad (30)$$

where

$$\tilde{I}^\pm = k^{\pm 2} + \iint_{\mathcal{D}} \phi_y^{\pm 2} + (1 - 3\omega^2)B^{-2}b^{-2}\phi_z^{\pm 2} dA. \quad (31)$$

Comparing (29) and (30) shows that the WKB representations break down in the neighbourhood of the transition (or turning) points where $C_g^\pm = 0$, denoted here by $\pm \xi_c$. Therefore in the interval $(-\xi_c, \xi_c)$ (excluding regions of width of $\varepsilon^{2/3}$ near the endpoints, Bender and Orszag, 1978) the first-order WKB solution is a superposition of the forward and backward propagating waves given by

$$\begin{aligned} \psi(\xi, y, z) = & \alpha f_0^- \phi^-(\xi, y, z) \exp \left\{ P(\xi) - \frac{i}{\varepsilon} \int_{-\xi_c}^{\xi} Q(\xi') d\xi' \right\} \\ & + \beta f_0^+ \phi^+(\xi, y, z) \exp \left\{ P(\xi) + \frac{i}{\varepsilon} \int_{-\xi_c}^{\xi} Q(\xi') d\xi' \right\}, \end{aligned} \quad (32)$$

where

$$P(\xi) = \frac{i}{2\varepsilon} \int_{-\xi_c}^{\xi} [k^+(\xi') + k^-(\xi')] d\xi', \quad Q(\xi) = \frac{1}{2} [k^+(\xi) - k^-(\xi)]. \quad (33)$$

The solution decaying in $\xi < -\xi_c$ is

$$\psi(\xi, y, z) = C_1 f_0^- \phi^-(\xi, y, z) \exp \left\{ P(\xi) - \frac{1}{\varepsilon} \int_{\xi}^{-\xi_c} |Q(\xi')| d\xi' \right\}. \quad (34)$$

It remains to be connected (32)–(34) across the turning point at $\xi = -\xi_c$. In classical WKB applications the counter-propagating waves in the allowed region sum to give a standing wave. Here however the waves in (32) have different offshore structures and it is only sufficiently close to $\xi = -\xi_c$ (and $\xi = \xi_c$) that they can be superposed. In the interval $\varepsilon^\gamma > \xi - (-\xi_c) > \varepsilon^{2/3}$ (so (32) remains valid), where $\gamma < 2/3$, $|\xi - (-\xi_c)|$ is small so $Q^2(\xi) \sim a(\xi - (-\xi_c))$ for some $a > 0$. Therefore $S^{\pm'} \sim k(-\xi_c) \pm a^{1/2}(\xi - (-\xi_c))^{1/2}$, and

$$A^\pm + B^\pm - 2\omega S^{\pm'} \sim \mp 2\omega a^{1/2}(\xi - (-\xi_c))^{1/2}. \quad (35)$$

Hence

$$f_0^\pm \phi^\pm \sim |2\omega a^{1/2}(\xi - (-\xi_c))^{1/2}|^{-1/2} \phi(-\xi_c, y, z) \quad (36)$$

and (32) reduces, at leading order, to

$$|2\omega a^{1/2}(\xi - (-\xi_c))^{1/2}|^{-1/2} \phi(-\xi_c, y, z) \exp \{ P(-\xi_c) \left(\beta \exp \left\{ \frac{i}{\varepsilon} \int_{-\xi_c}^{\xi} Q(\xi') d\xi' \right\} + \alpha \exp \left\{ -\frac{i}{\varepsilon} \int_{-\xi_c}^{\xi} Q(\xi') d\xi' \right\} \right). \quad (37)$$

Now the connection formula across $\xi = -\xi_c$, obtained directly from a consideration of Stokes and anti-Stokes lines by Berry and Mount (1972), determines the constants α and β as

$$\alpha = C_1 \exp(i\pi/4), \quad \beta = C_1 \exp(-i\pi/4). \quad (38)$$

More detailed considerations in the neighbourhood of turning points by Berry and Mount (1972) and Bender and Orszag (1978) show that the solution then forms an Airy front with the equivalent composite form here being

$$\begin{aligned} \psi(\xi, y, z) = & \omega^{-1/2} C_1 (2\pi)^{1/2} (ae)^{-1/6} \text{Ai} \{ -\varepsilon^{-2/3} a^{1/3} (\xi - (-\xi_c)) \} \\ & \times \phi(-\xi_c, y, z) \exp \{ P(-\xi_c) \}, \end{aligned} \quad (39)$$

where Ai is the Airy function of the first kind, smoothly matching (34)–(37) with α and β as in (38).

The solution decaying in $\xi > \xi_c$ is given by

$$\psi(\xi, x, y) = C_2 f_0^+ \phi^+(\xi, y, z) \exp \left\{ P(\xi) - \frac{1}{\varepsilon} \int_{\xi_c}^{\xi} |Q(\xi')| d\xi' \right\}. \quad (40)$$

Considerations identical to those of (35)–(37) over the interval $-\varepsilon^\gamma < \xi - \xi_c < -\varepsilon^{2/3}$ allow the propagating solution (32) to be connected to (40) across the turning point at $\xi = \xi_c$, giving the constraint

$$\frac{1}{\varepsilon} \int_{-\xi_c}^{\xi_c} Q(\xi') d\xi' \sim \left(n + \frac{1}{2} \right) \pi + O(\varepsilon), \quad n = 0, 1, 2, \dots \quad (41)$$

and $C_2 = (-1)^n C_1$, for n from (41). Since Q and ξ_c depend on ω equation (41) determines the frequency of the ℓ CTW of along-shore mode number n , as required. A composite Airy form equivalent to (39) again matches across $\xi = \xi_c$.

One immediate result from (41) comes from noting that the integral in (41) approaches its maximum value as $\xi_c \rightarrow \infty$ (i.e. $\omega \rightarrow \omega_c$ where ω_c is the cut off frequency at $\xi = \infty$) fixing the total number of trapped modes as

$$n \leq \frac{1}{\pi \varepsilon} \lim_{|\xi_c| \rightarrow \infty} \int_{-\xi_c}^{\xi_c} Q(\xi') d\xi' - \frac{1}{2}. \quad (42)$$

4. Arbitrary coastal geometries

Following JR, recast system (12) into a linear eigenvalue problem by writing

$$q = \lambda p \quad \text{and} \quad r = \lambda q, \quad (43)$$

where $\lambda = i\omega$ and map to a rectangular flow domain by introducing the vertical stretching

$$\xi = \varepsilon x, \quad \eta = y, \quad \theta = z\mu(\varepsilon x, y), \quad \text{where } \mu = 1/h(\varepsilon x, y). \quad (44)$$

Then the governing equations become

$$\varepsilon^2 p_{\xi\xi} + p_{\eta\eta} + 2(\varepsilon^2 \theta_{\xi} p_{\xi 0} + \theta_{\eta} p_{\eta 0}) + (\varepsilon^2 \theta_{\xi\xi} + \theta_{\eta\eta}) p_0 + (\varepsilon^2 \theta_{\xi}^2 + \theta_{\eta}^2) p_{00} + B^{-2} \mu (b^{-2} \mu p_0)_0 = -\lambda B^{-2} \mu (b^{-2} \mu q_0)_0, \quad (45a)$$

$$\varepsilon [h_{\eta} (p_{\xi} + \theta_{\xi} p_0) - h_{\xi} (p_{\eta} + \theta_{\eta} p_0)] = \lambda [b^{-2} B^{-2} \mu p_0 + \varepsilon^2 h_{\xi} (p_{\xi} + \theta_{\xi} p_0) + h_{\eta} (p_{\eta} + \theta_{\eta} p_0) + b^{-2} B^{-2} \mu r_0] \quad (\theta = -1, \eta \leq 1), \quad (45b)$$

$$\varepsilon (p_{\xi} + \theta_{\xi} p_0) = \lambda (p_{\eta} + \theta_{\eta} p_0) \quad (\eta = 0), \quad (45c)$$

$$p_0 = 0 \quad (\theta = 0), \quad (45d)$$

$$p_0 = 0 \quad (\theta = -1, \eta > 1), \quad (45e)$$

$$\nabla p \rightarrow 0, \quad \xi^2 + \eta^2 \rightarrow \infty, \quad (45f)$$

where

$$\theta_{\xi} = \mu_{\xi} \theta / \mu, \quad \theta_{\eta} = \mu_{\eta} \theta / \mu, \quad \theta_{\xi\xi} = \mu_{\xi\xi} \theta / \mu, \quad \theta_{\eta\eta} = \mu_{\eta\eta} \theta / \mu. \quad (46)$$

System (45) is a linear eigenvalue problem for λ . It can be solved accurately by extending the method in JR to three dimensions. System (45) is approximated pseudo-spectrally, by forming the 3D tensor product grid of N Chebyshev points, θ_i , in the vertical, M Laguerre points, η_j , offshore and K Hermite points, ξ_k , alongshore. The unknown values of p on the grid, taken in lexicographical order, then form a vector \mathbf{p} of size NMK . Following JR, form the discrete version of (45a) using differentiation matrices and replace rows corresponding to boundary points with the corresponding discrete forms of the boundary conditions (45b)–(45e) gives a $3NMK \times 3NMK$ generalised linear algebraic eigenvalue problem

$$\begin{pmatrix} \mathbf{A} & \mathbf{0} & \mathbf{0} \\ \mathbf{0} & \mathbf{I} & \mathbf{0} \\ \mathbf{0} & \mathbf{0} & \mathbf{I} \end{pmatrix} \begin{pmatrix} \mathbf{p} \\ \mathbf{q} \\ \mathbf{r} \end{pmatrix} = \lambda \begin{pmatrix} \mathbf{B} & \mathbf{C} & \mathbf{D} \\ \mathbf{I} & \mathbf{0} & \mathbf{0} \\ \mathbf{0} & \mathbf{I} & \mathbf{0} \end{pmatrix} \begin{pmatrix} \mathbf{p} \\ \mathbf{q} \\ \mathbf{r} \end{pmatrix}, \quad (47)$$

where \mathbf{I} is the $NMK \times NMK$ identity matrix and $\mathbf{0}$ is the $NMK \times NMK$ null matrix. The accuracy and speed of the numerical solution of (47) can be greatly increased by using the accurate WKBJ eigenvalues as an initial estimate for an inverse iteration. Write $\lambda = \lambda_0 + \tilde{\lambda}$, where λ_0 is the WKBJ estimate for λ , so $\tilde{\lambda} \ll 1$. The generalised linear eigenvalue problem can formally be written as the more familiar regular eigenvalue problem

$$\mathbf{E} \mathbf{q} = \tilde{\lambda} \mathbf{q}, \quad (48)$$

where

$$\mathbf{E} = \begin{pmatrix} \mathbf{A} - \lambda_0 \mathbf{B} & -\lambda_0 \mathbf{C} & -\lambda_0 \mathbf{D} \\ -\lambda_0 \mathbf{I} & \mathbf{I} & \mathbf{0} \\ \mathbf{0} & -\lambda_0 \mathbf{I} & \mathbf{I} \end{pmatrix}^{-1} \begin{pmatrix} \mathbf{B} & \mathbf{C} & \mathbf{D} \\ \mathbf{I} & \mathbf{0} & \mathbf{0} \\ \mathbf{0} & \mathbf{I} & \mathbf{0} \end{pmatrix}, \quad \mathbf{q} = \begin{pmatrix} \mathbf{p} \\ \mathbf{q} \\ \mathbf{r} \end{pmatrix} \quad (49)$$

and $\tilde{\lambda} = 1/\hat{\lambda}$, so $\tilde{\lambda} \gg 1$. For the standard forward iteration

$$\hat{\mathbf{q}}_{j+1} = \mathbf{E} \mathbf{q}_j, \quad \mathbf{q}_{j+1} = \hat{\mathbf{q}}_{j+1} / \sigma_{j+1}, \quad (50)$$

where σ_{j+1} is a normalising factor for $\hat{\mathbf{q}}_{j+1}$, chosen here to be the element of $\hat{\mathbf{q}}$ of largest absolute value, the sequence σ_j converges to the largest eigenvalue of \mathbf{E} , here $\tilde{\lambda}$ by construction. It is not necessary to calculate \mathbf{E} explicitly to implement this scheme. Instead, (48) can be rearranged as

$$(\mathbf{A} - \lambda_0 \mathbf{B} - \lambda_0^2 \mathbf{C} - \lambda_0^3 \mathbf{D}) \hat{\mathbf{p}}_{j+1} = (\mathbf{B} + \lambda_0 \mathbf{C} + \lambda_0^2 \mathbf{D}) \mathbf{p}_j + (\mathbf{C} + \lambda_0 \mathbf{D}) \mathbf{q}_j + \mathbf{D} \mathbf{r}_j, \quad (51)$$

$$\hat{\mathbf{q}}_{j+1} = \hat{\mathbf{p}}_{j+1} + \lambda_0 \mathbf{p}_j, \quad (52)$$

$$\hat{\mathbf{r}}_{j+1} = \hat{\mathbf{q}}_{j+1} + \lambda_0 \mathbf{q}_j. \quad (53)$$

For appropriate initial estimates λ_0 , \mathbf{p}_0 , \mathbf{q}_0 and \mathbf{r}_0 , Eq. (51) is a standard set of NMK linear equations of the form $\mathbf{A} \mathbf{x} = \mathbf{b}$, which can be solved by standard means. In particular the matrix on the left hand side of (51) can be factorised once and for all at the beginning of any computation, and subsequent inversions of (51) reduce to back substitution. In all subsequent numerical results, presented here, N , M and K have been chosen sufficiently large so that the eigenvalues are resolution independent at the stated accuracy.

5. Geometric and stratification effects on localised modes

5.1. Shelf geometries

Consider the non-rectilinear depth profile in $y \geq 0$ and $|x| < \infty$, normalised to give unit depth at $y=0$ and $y=1$, given by

$$\hat{h}(x, y) = 1 - [1 - d(\varepsilon x) H_0] \exp\left\{-\frac{ay}{(1-y)}\right\} \left\{1 - \tanh\left[\frac{y - \sigma(\varepsilon x)}{\delta(\varepsilon x)}\right]\right\} / 2, \quad (54)$$

where $d = [1 - 2H_0 + \tanh(-\sigma/\delta)] / [H_0 \tanh(-\sigma/\delta) - H_0]$, H_0 is the depth at the coast, a measures the gradient of the shelf slope, σ gives the distance of the shelf break from the coast and δ measures the slope of the shelf break. Various forms for the longshore variation σ and δ are discussed below. In all computations the shelf width to alongshore variation is taken to be $\varepsilon = 0.1$.

5.2. Local CTW dispersion properties

As CTWs propagate along shelves with slow longshore variations in bottom topography or coastline curvature it is the local structure of the waves that determine the existence of ℓ CTWs. Huthnance (1978) shows that at short wavelengths the frequency of all CTWs approaches the same value, ω_{∞} say, where

$$\omega_{\infty} = \lim_{k \rightarrow \infty} \omega = B \max_k [b(z) dh/dy]_{z=-h(y)}. \quad (55)$$

For a given profile there is thus a critical stratification parameter B^c given by

$$(B^c)^{-1} = \max_k [b(z) dh/dy]_{z=-h(y)}, \quad (56)$$

such that dispersion curves pass through f for stratification $B > B^c$, but fail to reach f for stratification $B < B^c$. For strong stratification where $B > B^c$ everywhere, energy propagates unidirectionally and no ℓ CTWs exist. For weaker stratification, where $B < B^c$ somewhere, the group velocity changes sign and energy can propagate in both directions. Typical dispersion curves for different values of B with b constant are shown in Fig. 2 for the wide shelf break (at $x=0$) shown in Fig. 1(a). For weak stratification dispersion curves have at least one turning point, where ω has a local maximum (Fig. 2(a)). There is also an intermediate range of stratification, where in addition to a local maximum, $\omega(k)$ may also have a local minimum. This intermediate regime is discussed in more detail below.

5.3. Perturbations in shelf-break distance

5.3.1. Conditions for trapping

Fig. 2 shows the dispersion relation for the widening shelf of Fig. 1(a,b) following JR. As expected, the increase in shelf-break distance, i.e. the weakening of the coastal constraint (Johnson and Kaoullas, 2011) in the neighbourhood of the origin raises the maximum frequency for propagating CTWs. For sufficiently low stratification the flow is essentially barotropic and the local dispersion relations in Fig. 2(a) have a single maximum for ω . Let $\omega_{c, \text{far}}^m$ be the frequency of mode m at the local maximum for the far field shelf geometry at $|x| = \infty$, and $\omega_{c, \text{local}}^m$ the

corresponding frequency for the locally perturbed shelf at $x=0$. For intermediate stratifications there may also exist a local minimum for ω . For $B=0.2$ the local minimum $\omega_{c,far}^{1,*}$ of mode 1 for the far field geometry is clearly visible in Fig. 2(b). This local minimum gives the lowest frequency for which a particular mode has a negative group velocity. For $B=0.01$ (see Fig. 2(a)), it is clear that $\omega_{c,far}^m < \omega_{c,local}^m$ for modes 1 and 2, and ω_∞ gives the lower bound for waves with negative group velocity. Therefore a CTW with frequency ω_m , with $\omega_{c,far}^m < \omega_m < \omega_{c,local}^m$, propagates locally to the wide shelf, but is cut-off in the far field.

With increasing stratification there is a qualitative change in the waves. For the localised widening of the shelf given by the depth profile shown in Fig. 1(a,b), there is no longshore variation in the value of $\max h_y|_{z=-h(y)}$. Thus, from (55), for uniform stratification, only changes in B affect ω_∞ : for a given B all modes have the same limiting frequency ω_∞ at each point along the coast, as in Fig. 2(b). For mode 2, ω_∞ is now the maximum frequency of propagation everywhere. Thus for waves with frequency $\omega < \omega_\infty$ energy propagation is strictly unidirectional and mode 2 is not localised on this profile. The qualitative behaviour of mode 1 remains the same as for Fig. 2(a).

Comparing the limiting frequency ω_∞ and local maximum frequency as a function of stratification for the two profiles gives a clearer demonstration of the importance of these limiting frequencies on the existence of trapped modes. Fig. 3(a) shows the variation of the local maximum (solid lines) and limiting frequency ω_∞ (dashed lines) for the two limiting shelf topographies as a function of stratification (for $b(z)$ constant). The shaded areas show the range of stratification where trapping is possible, and the lower and upper bounds of the trapped mode frequencies, i.e. a frequency within the grey shaded region is greater than the maximum frequency of propagation in the far field and is therefore cut-off. The same frequency on the local wide section is less than the local maximum, and therefore energy propagates in both directions. Since higher modes have lower frequencies (Huthnance, 1978), the range of stratifications for which the maximum frequency of propagation on the wide shelf is above the limiting frequency ω_∞ is smaller for higher modes and so ℓ CTWs exist over smaller ranges of stratification. Fig. 3(a) shows the range for possible trapping of mode 1 extends to $B \simeq 0.2$, whereas for mode 2 it extends to only $B \simeq 0.1$. In general, for a given stratification, localisation of mode n requires

$$\max(\omega_\infty, \omega_{c,far}^m) < \omega_{c,local}^m \quad (57)$$

The frequencies $\omega_{c,local}^m$ and $\max(\omega_\infty, \omega_{c,far}^m)$ then give upper and lower bounds for the trapped mode frequency respectively.

5.3.2. Trapped modes

ℓ CTWs can be characterised by their cross-shelf mode number m and their along-shore mode number n . Denote the frequency of the (n,m) mode by $\omega_{n,m}$. Six digit accuracy is achieved for mode $\omega_{0,1}$ with $B=0.01$, $b(z) \equiv 1$, $N=8$, $M=34$ and $K=34$, computed as in Section 4. Higher modes require more grid points for comparable accuracy. Fig. 4 shows the real parts of $p(x,y,-h)$ of the bottom pressure for modes $\omega_{0,1}$ and $\omega_{0,2}$ at $B=0.01$. The offshore structure of the modes follows Huthnance (1978) with the number of zero crossings equal to the mode number, and the largest displacement found near the coast.

Table 1 gives the comparison between the WKBJ and numerical eigenvalues. Constraint (41) was solved combining Gaussian quadrature with an adaptive secant root finding algorithm to determine the frequency ω . Since the integral constraint is symmetric, for the chosen profiles, it is sufficient to consider only the range $[0, \xi_c]$. Accuracy is further improved by removing the square root singularity in Q , at $\xi = \xi_c$, through the change of variable $\chi = (\xi - \xi_c)^{1/2}$. The function $Q(\xi)$ at each Gaussian point

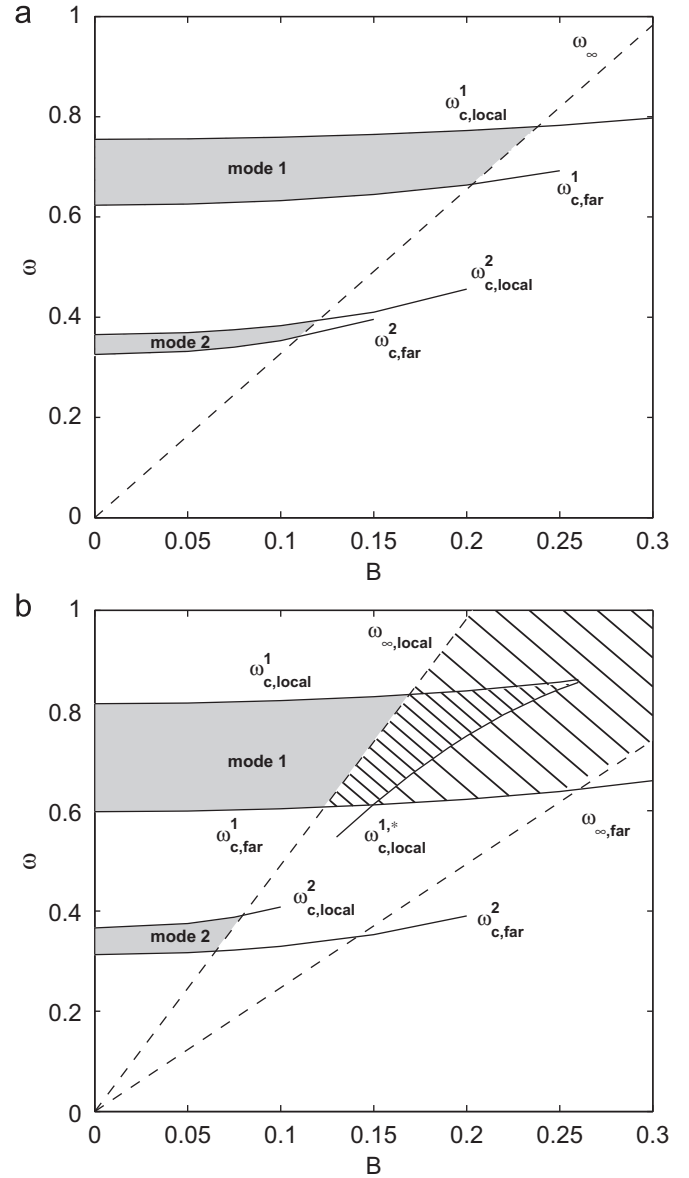


Fig. 3. Trapping regime with $b(z) \equiv 1$ for modes 1 and 2 over the topography of (a) Fig. 1(a,b) and (b) Fig. 1(c,d). The shaded regions give the values of B where trapped modes are possible. Details of the closely hatched region are included in Fig. 6.

along the coast is obtained rapidly and accurately using inverse iteration as in JR, with initial guess linearly extrapolated from the portion of the function $Q(\xi)$ already determined. The eigenvalues thus obtained in each cross section are accurate to nine significant figures and comparable accuracy for the ℓ CTW frequency requires only 10 Gaussian points. The WKBJ determined frequencies are accurate to within a 10th of a percent with accuracy increasing with offshore and alongshore mode numbers. The agreement with the full numerical solution even for this modest ε is remarkable.

5.4. Perturbations in shelf slope

For a shelf whose slope increases locally, as the depth profile of 1(c,d), the limiting frequency ω_∞ varies as a function of both the stratification and position along the shelf, giving parameter ranges with more complicated variations in dispersion relations. Fig. 5 shows typical dispersion relations. The local minimum for mode 1 in the steep section at $B=0.15$ is labeled $\omega_{c,local}^{1,*}$ in

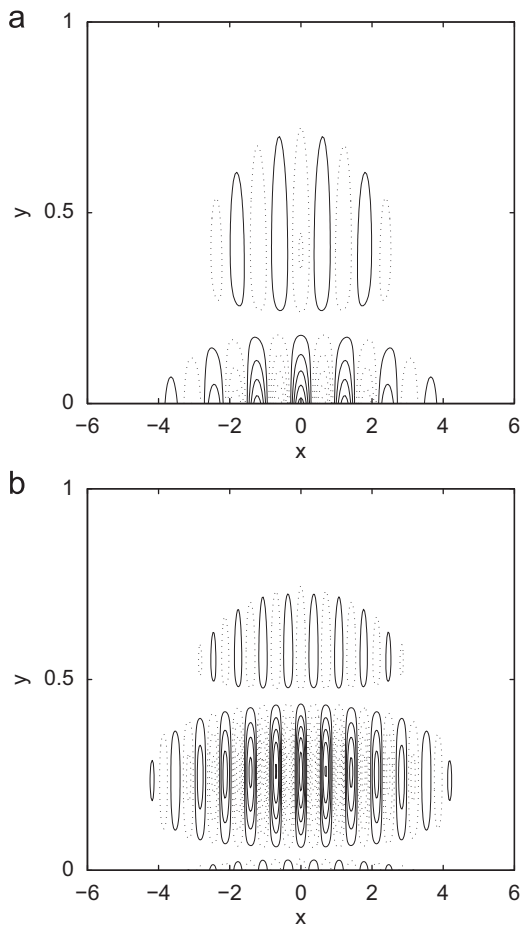


Fig. 4. The real part of the bottom pressure $p(x,y,-h)$ for (a) the fundamental ℓ CTW mode $\omega_{0,1}$ and (b) the ℓ CTW mode $\omega_{0,2}$ for the depth profile 1(a,b) with $B=0.01$ and $b(z)\equiv 1$. The contours are at equal intervals with negative values dashed and the zero contour omitted.

Table 1

The eigenfrequencies $\omega_{n,m}^A$ from the WKB method and the numerical eigenfrequencies $\omega_{n,m}^N$ for the topography of Fig. 1(a,b), for various modes and stratification B with $b(z)\equiv 1$.

n	m	B	$\omega_{n,m}^A$	$\omega_{n,m}^N$	Error (%)
0	1	0.01	0.7518365	0.7519881	0.0201
1	1	0.01	0.7454791	0.7456205	0.0190
2	1	0.01	0.7393040	0.7394385	0.0182
0	1	0.15	0.7615593	0.7616983	0.0182
1	1	0.15	0.7555876	0.7557198	0.0175
2	1	0.15	0.7497965	0.7499211	0.0166
0	2	0.01	0.3647694	0.3647729	0.0009
1	2	0.01	0.3640451	0.3640447	0.0001

Fig. 5(b). Fig. 3(b) gives the variation of the cut-off frequencies, the limiting frequencies ω_∞ and the local minimum $\omega_{c,\text{local}}^{1,*}$ as a function of B , at uniform stratification, for the shelf profile given by Fig. 1(c,d). The shaded regions, again show the permitted regimes where CTWs are evanescent in the far field and have bi-directional group velocity above the steep section—a necessary requirement for ℓ CTWs. At frequencies within the narrow hatched region of Fig. 3(b) mode 1 is evanescent in the far field, but propagates as a superposition of three transverse waves on the steep shelf: two waves of comparable wavelength close to the local maximum and a comparatively shorter wave, shorter than the wavelength at the local minimum. Since the modes are evanescent in the far field they can superimpose to form a

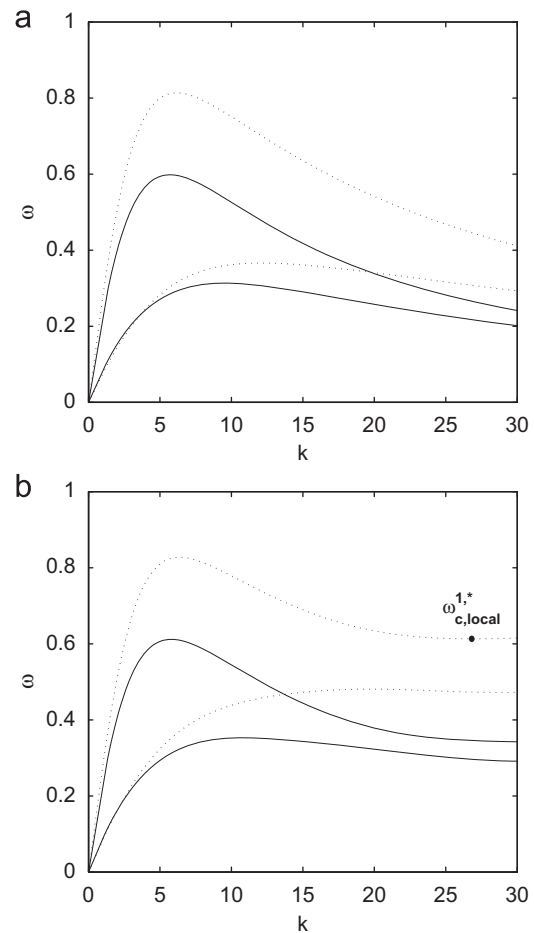


Fig. 5. Dispersion curves for modes 1 and 2 over steep shelf (dashed line) and the far field shelf (solid line) depth profiles shown in Fig. 1(c,d) at uniform stratification with (a) $B=0.01$ and (b) $B=0.15$.

trapped mode. Even though the WKB approximation omits the shortest locally propagating mode, the WKB frequencies once again agree closely with numerical solutions to the full problem found by continuation, gradually increasing the stratification from a known asymptotic solution (in the shaded region). The crosses in Fig. 6 show the converged (to six digit accuracy) numerical eigenfrequencies $\omega_{0,1}$ that lie close to or within the hatched region of Fig. 3(b), as a function of the stratification B (for $b(z)\equiv 1$).

A mode with a frequency within wide hatched region of Fig. 3 propagates as a mode with uni-directional group velocity on the steep shelf but is cut-off in the far field. A similar uni-directional topographic wave problem in Johnson (1985) shows that energy accumulates in singular regions when wave reflection is not possible. An and McDonald (2005) show that nonlinearity leads to eddy shedding from these regions. Similar effects can be expected in this particular parameter regime of the current problem. Fig. 7(a) shows the real part $p(x,y,-h)$ of the bottom pressure for the fundamental ℓ CTW for the depth profile shown in 1(c,d) at $B=0.25$. The along-shore extent of the mode is smaller here, at higher stratification, than for the equivalent ℓ CTW of Fig. 4.

6. Discussion

Localised coastal trapped waves, ℓ CTWs, have been constructed for a continuously stratified shelf abutting a constant

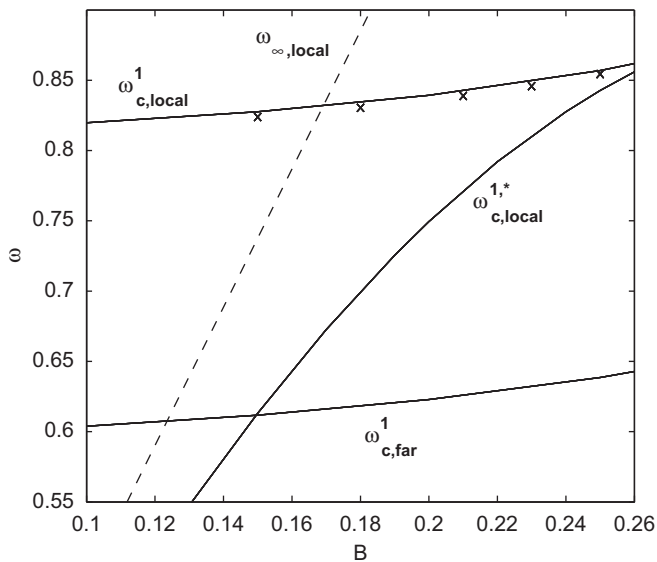


Fig. 6. The fundamental l CTW frequency, denoted by the crosses, as a function of B for the topography shown in Fig. 1(c,d).

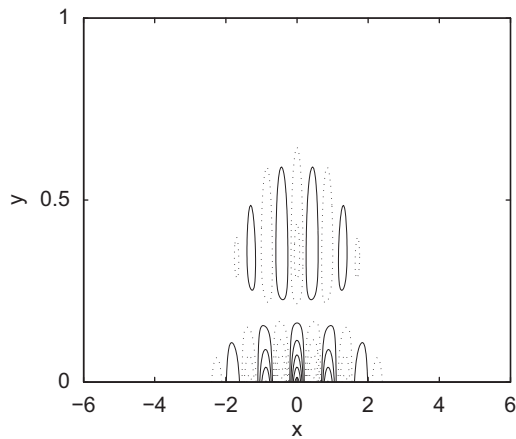


Fig. 7. The real part $p(x,y,-h)$ of the bottom pressure for the fundamental l CTW mode $\omega_{0,1}$ as a function of x and y at $z = -h(x,y)$, for the depth profile 1(c,d) with $B=0.25$ and $b(z)$ held constant.

depth ocean, both semi-analytically for slowly-varying shelves and numerically for arbitrary variations. The two methods show remarkable agreement. Considering the local dynamics of CTWs shows that the important parameters governing the existence of l CTWs are the stratification, shelf slope and the distance of the shelf break from the coastal wall. l CTWs occur for a wider range of parameters when the coastal constraint is locally weakened by the shelf-break moving further offshore, when the shelf steepens and when stratification is weaker. l CTWs are the superposition of two CTWs carrying energy in opposite directions and so in regions of parameter space where bi-directional energy propagation is not possible no l CTWs exist. In parameter regimes where a CTW propagates uni-directionally towards a section of shelf where that mode is evanescent, the incident CTW energy may be converted to eddy motion.

The present analysis extends the localised barotropic shelf wave theory to include stratification and constructs l CTWs for stratification for $B \lesssim 0.25$. The l CTWs have little vertical structure and so would not be sensitive to vertical resolution in coastal-ocean models. However, it would seem that model simulation of

l CTWs would require sufficient horizontal resolution to capture longshore topographic variations and the offshore decay of the modes.

Since energy absorbed by l CTWs cannot propagate away the l CTW frequencies may appear as pronounced peaks in low frequency spectra of coastal flows. Observations on the Scotian shelf (Schwing, 1989) show that the frequency of energetic disturbances near the Laurentian channel are higher than those of propagating modes on the shelf, consistent with localised trapping in the estuary region (Stocker and Johnson, 1991). Similarly topographic variations in lakes appear to allow localised modes. Modes concentrated at lake ends have been found numerically in both the finite-element model of the lake of Laguno (Trösch, 1986) and the rectangular basin with variable, but symmetric, topography model of Stocker and Hutter (1987). Johnson and Kaoullas (2011) use a simple geometrical lake-end bay model to attribute these localised bay-modes to geographically localised topographic waves. The inclusion of a flat bay raises the frequency of the locally propagating waves at the lake-end and modes exist that propagate in the neighbourhood of the bay region but decay exponentially in the far-field. The present results suggest that l CTWs could be observed in the neighbourhood of local coastal geometric variations, such as increases in shelf slope, shelf break distance or curvature, which raise the maximum allowable frequency of propagation.

Acknowledgments

JTR was supported by the NERC research studentship NE/F008260/1 from the National Oceanography Centre, Liverpool.

References

- Adamou, A., Craster, R., Llewellyn Smith, S., 2007. Trapped edge waves in stratified rotating fluids: numerical and asymptotic results. *Journal of Fluid Mechanics* 592, 195–220.
- An, B.W., McDonald, N.R., 2005. Coastal currents and eddies and their interaction with topography. *Dynamics of Atmospheres and Oceans* 40, 237–253.
- Bender, C., Orszag, S., 1978. *Advanced Mathematical Methods for Scientist and Engineers*, second ed. McGraw-Hill, New York.
- Berry, M., Mount, K., 1972. Semiclassical approximation in wave mechanics. *Reports on Progress in Physics* 35, 315–397.
- Heading, J., 1962. *An Introduction to Phase Integral Methods*. Methuen and Co, London.
- Huthnance, J.M., 1978. On coastal trapped waves-analysis and numerical calculation by inverse iteration. *Journal of Physical Oceanography* 8 (1), 74–92.
- Johnson, E.R., Kaoullas, G., 2011. Bay-trapped low-frequency oscillations in lakes. *Geophysical and Astrophysical Fluid Dynamics* 105 (1), 48–60.
- Johnson, E.R., Rodney, J.T., 2011. Spectral methods for coastal trapped waves. *Continental Shelf Research* 31 (14), 1481–1489.
- Johnson, E.R., 1985. Topographic waves and the evolution of coastal currents. *Journal of Fluid Mechanics* 160, 499–509.
- Johnson, E.R., Levitin, M., Parnowski, L., 2006. Existence of eigenvalues of a linear operator pencil in a curved waveguide-localised shelf waves on curved coast. *SIAM Journal on Mathematical Analysis* 32 (5), 1465–1481.
- Johnson, E.R., Rodney, J.T., Kaoullas, G., 2011. Trapped modes in coastal waveguides. *Wave Motion*. doi:10.1016/j.wavemoti.2011.08.004, in press.
- Kaoullas, G., Johnson, E.R., 2010. Geographically localised shelf waves on curved coasts. *Continental Shelf Research* 30 (16), 1753–1760.
- Postnova, J., Craster, R., 2008. Trapped modes in elastic plates, ocean and quantum waveguides. *Wave Motion* 45, 565–579.
- Schwing, F.B., 1989. Subtidal response of the Scotian shelf bottom pressure field to meteorological forcing. *Atmosphere-Ocean* 27, 157–180.
- Stocker, T.F., Hutter, K., 1987. Topographic waves in rectangular basins. *Journal of Fluid Mechanics* 185, 107–120.
- Stocker, T.F., Johnson, E.R., 1991. The trapping and scattering of topographic waves by estuaries and headlands. *Journal of Fluid Mechanics* 222, 501–524.
- Trösch, T., 1986. Finite element calculation of topographic waves in lakes. In: Hsia, H.M., Chou, Y.L., Wang, S.Y., Hsieh, S.J. (Eds.), *Proceedings of the Fourth International Conference on Applied Numerical Modeling* (Taiwan, Taiwan, 1984), Science and Technology Series, vol. 63. American Astronautical Society, pp. 307–311.